Design and Comparison of Resonant and Non-Resonant Single-Layer Microwave Heaters for Continuous Flow Microfluidics in Silicon-Glass Technology

Tomislav Markovic [1,2,*], Ilja Ocket [1,2], Adrijan Baric [3] and Bart Nauwelaers [2]

1   IOT Group, imec, Kapeldreef 75, 3001 Heverlee, Belgium; ilja.ocket@imec.be
2   Division TELEMIC, Department of Electrical Engineering (ESAT), KU Leuven, Kasteelpark Arenberg 10, 3001 Leuven, Belgium; bart.nauwelaers@kuleuven.be
3   Department of Electronics, Microelectronics, Computer and Intelligent Systems, Faculty of Electrical Engineering and Computing, University of Zagreb, Unska 3, 10000 Zagreb, Croatia; adrijan.baric@fer.hr
*   Correspondence: tomislav.markovic@kuleuven.be; Tel.: +32-16-32-96-89

check for updates

Abstract: This paper presents a novel concept for the co-design of microwave heaters and microfluidic channels for sub-microliter volumes in continuous flow microfluidics. Based on the novel co-design concept, two types of heaters are presented, co-designed and manufactured in high-resistivity silicon-glass technology, resulting in a building block for consumable and mass-producible micro total analysis systems. Resonant and non-resonant co-planar waveguide transmission line heaters are investigated for heating of sub-micro-liter liquid volumes in a channel section at 25 GHz. The heating rates of 16 and 24 °C/s are obtained with power levels of 32 dBm for the through line and the open-ended line microwave heater, respectively. The heating uniformity of developed devices is evaluated with a Rhodamine B and deionized water mixture on a micrometer scale using the microwave-optical measurement setup. Measurement results showed a good agreement with simulations and demonstrated the potential of microwave heating for microfluidics.

Keywords: microwave heating; microfluidics; silicon; chip integration

1. Introduction

Microfluidic devices enable various applications through incorporated technological functions on a chip, as illustrated in Figure 1. In lab-on-a-chip systems, microfluidic mixers are often achieved using meandered channels [1] or ridges in a channel [1]. Liquid filtering and particle separation are achieved using microfluidic filters with an array of pillars [2], while signal detection to evaluate reactions is done using optical [3] or electrical devices [4–6]. Temperature control is achieved utilizing contact-based heating devices [7]. The traditional heaters perform adequately if thermal runaway to the whole fluidic device is not a limiting factor, and the substrate material of the fluidic chip can conduct heat sufficiently well. If one of these two factors cannot be respected, a different heating technique is required.

An alternative solution for temperature control is microwave heating as it does not rely its operation on heat conduction—heat is generated by the liquid itself once it is exposed to an alternating electric field. Several research groups have reported microwave heating devices [8–18] for digital and continuous microfluidics in the past decade. For continuous flow microfluidics, the focus has been on heating of individual pico- and nano-liter droplets flowing through fluidic channels [8–12], microliter volumes in wells placed along fluidic channels [13,14], or on heating of liquid located over the complete fluidic chip [15,16]. Although all reported devices present breakthroughs in their fluidic

subdomains, they cannot be entirely applied and up- or down-scaled to heat the liquid located in a section of a channel section on a planar fluidic chip, as illustrated in Figure 1. In summary, the reported investigations dealt with two extreme points concerning the liquid volume—individual droplets or relatively large individual reservoirs. In other words, a microwave heater investigation for sub-microliter volumes in continuous microfluidics has been lagging so far.

Thus, this work investigates the possibilities of microwave heaters for sub-microliter volumes located in a channel section in a continuous flow microfluidic chip, as illustrated in Figure 1, and the novelty of this work lies in a co-design of microwave heaters and microfluidic channels on a high-thermally conductive substrate, demonstrated by the design and evaluation of two types of microwave heaters. The investigated microwave devices provide uniform, contactless and localized microwave heating without restrictions on existing optical and fluidic techniques. All of this makes the novel microwave heating devices a basic building block that can be up- or down-scaled for the lab-on-a-chip systems. In our investigation, devices are realized in a single metal layer and integrated with a microfluidic chip in silicon-glass technology [19]. Alternatively, the proposed approach for the design of microwave heaters can be implemented in the standard printed circuit board (PCB) technology. Furthermore, the manufactured heater on a PCB can be further integrated with numerous fluidic devices manufactured using the established [20] or novel [21] fabrication processes and materials in microfluidics, such as glass, poly(methyl methacrylate) (PMMA) or polydimethylsiloxane (PDMS). Finally, complete versatility required nowadays in the lab-on-a-chip device development is fully achievable, given that the proposed microwave devices can be stacked up with existing microfluidic devices.

Previously, we reported the microwave characterization of manufactured devices on a die using the probe station and microwave ground-signal-ground (GSG) probes in conference proceedings [22,23]. Here, we present in detail the design approach of two types of devices, their comparison and integration with the supporting microwave circuitry, and finally, evaluation of heating performance on deionized water samples.
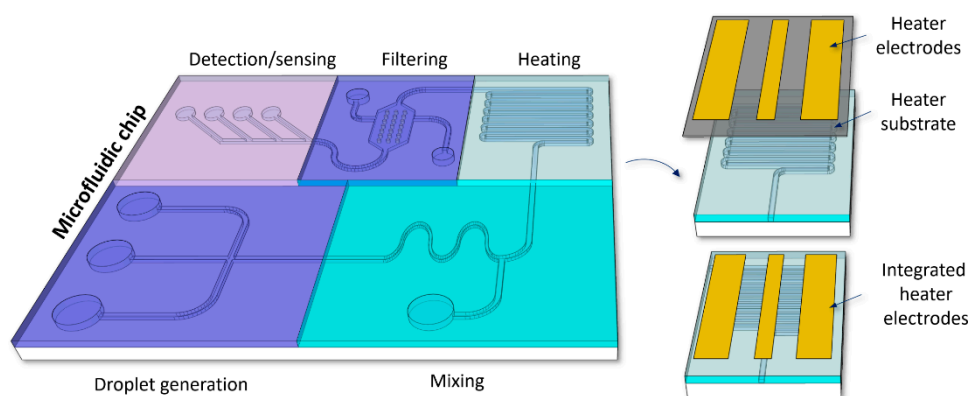

Figure 1. Microfluidic chip having several zones on the chip, incorporating functions such as droplet generation, liquid mixing, heating and filtering, and signal sensing. Microwave heaters can be implemented directly on top of the microfluidic device or can be implemented using the printed circuit board (PCB) technology and stacked-up with the microfluidic chip.

2. Materials and Methods

2.1. Device and System Fabrication and Integration

The microfluidic channels are micro machined in an 8 " high-resistivity (bulk = 10^{-5} S/cm) silicon (HR-Si) wafer (Topsil Semiconductor Materials A/S, Frederikssund, Denmark, part number 334-11000-0525-012), which is then bonded to a borosilicate glass wafer and subsequently singulated [19]. The height and width of the microfluidic channels are 100 and 240 μm, respectively, while the total

thickness of the HR-Si is 400 μm, as shown in Figure 2a. The cover glass thickness is 300 μm. The buried fluidic channels comprise a reaction chamber, as shown in Figure 2a. The purpose of trenches in the silicon substrate is to thermally isolate the reaction chamber from the rest of the device [19] due to the high thermal conductivity of silicon. Aluminum metal layer is on top of the HR-Si, in which heaters are realized.

To integrate the manufactured devices on HR-Si dies with the microwave laboratory equipment for evaluation, a Rogers PCB (Rogers Corporation, Evergem, Belgium, part number RO4350B) was used. The 254 μm thick substrate was selected together with the copper thickness of 35 μm, on top where a 25 μm thick gold/nickel metal layer was electroplated to enable further wire bonding of microwave heaters on HR-Si with feeding transmission lines on the PCB. For feeding transmission lines on the PCB, a grounded co-planar waveguide (GCPW) topology was selected. The vias connecting the top and bottom metal layers of the PCB are spaced 500 μm apart to avoid substrate mode losses at high microwave frequencies. Additionally, the 10-mil thick substrate was chosen as it allows 50 Ohm transmission line dimensions similar to dimensions of microwave heaters on HR-Si. The metal layers on HR-Si dies and the PCB were wire bonded using a HB16 wire bonder (TPT, Munich, Germany). To interconnect the wire bonded dies on the PCB with the microwave equipment, a high frequency end launch connectors (Johnson Cinch Connectivity-Bel Stewart GmbH, Friedrichsdorf, Germany, part number 142-0761-861) were soldered to the PCB. Finally, the obtained stack-up shown in Figure 2b was fixed to an acrylic glass holder—a 4 mm thick acrylic sheet was sized using a speedy 100R laser cutter (Trotec Laser, Haaksbergen, The Netherlands).
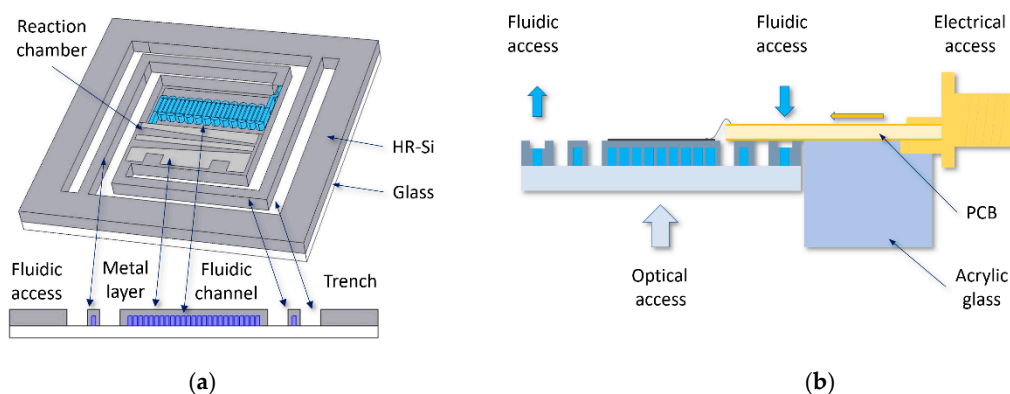

(**a**) (**b**)

Figure 2. Technology and stack-up overview: (**a**) The 3D and cross section view of the reaction chamber on a high-resistivity silicon (HR-Si) die with the aluminum metal layer on top and buried microfluidic channels covered with glass; (**b**) cross-section of the stack-up consisting of the HR-Si die, PCB and acrylic glass holder.

2.2. Heater Design and Integration

Microwave heaters are designed to heat the liquid located in a channel section, as illustrated in Figure 1. In our investigation, this channel section is located in a reaction chamber, as presented in Figure 2a. The reaction chamber with its fluidic inlet and outlet is a basic building block that can be used in any lab-on-a-chip design case, as simple as a fluidic mixer or a filter would be used. The size of the reaction chamber is fixed to 3.6×3.6 mm, and the fluidic channel dimensions of 100×240 μm are kept constant in the chamber. Microwave heaters can be realized in only one metal layer that comes on top of the fluidic substrate, as presented in a device cross section in Figure 2a. By maintaining this technological restriction in terms of the single metal layer, design versatility from an integration perspective is retained because the single metal layer can be placed on top of the fluidic substrate in multiple ways. Moreover, when the spacing between the buried channel in the fluidic chip and the single metal layer is present, contactless microwave heating is achieved. Additionally, placing

microwave heaters only over the reaction chamber results in localized microwave heating that does not heat the surrounding liquid on the fluidic chip.

To achieve uniform microwave heating, equal amounts of power should be dissipated over the liquid volume across the complete reaction chamber. To achieve this requirement, lossy microwave transmission lines are chosen because their physical implementation and corresponding dimensions can be designed in such a way that microwaves traveling along the line dissipate an equal amount of power in the liquid located in the reaction chamber. In this investigation, lossy transmission lines are realized using co-planar waveguides that consist of three electrodes in the single metal layer, as presented in Figure 2a. One electrode represents a central conductor of the co-planar waveguide line while the remaining two electrodes represent ground conductors of the transmission line. Other transmission line topologies such as microstrip or grounded co-planar waveguide could also be used at the cost of several metal layers, which does not comply with our initial requirement. Additionally, these transmission line technologies would restrict the optical access to the liquid located in the reaction chamber, which is not desired for the novel microwave-optical-fluidic platform.

Lossy co-planar waveguide transmission lines offer numerous possibilities in design and flexibility with respect to their size that is a limiting parameter in this investigation—a meticulous theoretical analysis of transmission lines is presented in textbook of D. Pozar [24]. In addition to the design possibilities, lossy microwave transmission lines allow two modes of heating—a traveling wave mode and a standing wave mode. In the traveling wave mode, microwaves travel along the line without any local reflections and exit the line at the output port that is terminated with 50 Ohm. In the standing wave mode, microwaves travel along the line without any local reflections but encounter a reflection at the end of the line because the output port is left open—from the transmission line theory, the open output port causes a reflection that is responsible for creating a standing wave along the line. In both modes of operation, the dissipated microwave power is given by Equation [24]:

$$P(z) = |V(z)|^2/Z_0, \tag{1}$$

in which $P(z)$ represents the amount of dissipated power along the line, $V(z)$ represents the voltage along the line and Z_0 represents the characteristic impedance of the line. Furthermore, the voltage along the line $V(z)$ can be expressed using the Equation [24]:

$$V(z) = V^+ \cdot e^{-\gamma z} \cdot (1 + \Gamma_L \cdot e^{2\gamma z}), \tag{2}$$

in which V^+ represents an incident wave entering the line, γ represents a propagation constant of the line, z represents the position along the line, and Γ_L represents the reflection coefficient of the load at the end of the line, given by:

$$\Gamma_L = (Z_L - Z_0)/(Z_L + Z_0), \tag{3}$$

In other words, the voltage (i.e., electric field) along the line responsible for microwave dielectric heating is a sum of two waves on the line, among which the reflected wave is caused by the mismatch between the characteristic impedance of the line (i.e., Z_0) and the load impedance (i.e. Z_L). Based on Equation (3), Γ_L is 0 in the traveling wave mode as the load impedance is chosen to be 50 Ohm and the characteristic impedance of the line is designed to be 50 Ohm. Moreover, this consequently results in a single term in Equation (2). In the standing wave mode, Γ_L is different from zero and preferably designed to be 1 or −1 to obtain large wave reflections. To obtain Γ_L of −1 or 1, we should keep the output port shorted or open, which consequently results in a very small or a very large impedance (i.e., 0 and ∞ Ohm, respectively). For the detailed analysis of microwave transmission line theory, we refer the reader to the textbook of D. Pozar [24].

In this investigation, we have chosen modes of heating having Γ_L close to 0 and 1. A heater having Γ_L close to 0 (the traveling wave mode) is a through line microwave heater (TLMH), while a heater having Γ_L close to 1 (the standing wave mode) is an open-ended line microwave heater (OELMH)

because an open circuit is used at the end of the transmission line. Both microwave heaters are designed at an operating frequency of 25 GHz. This choice is made to maximize the amount of dissipated power in the liquid in the fluidic channel caused by the presence of an electric field of microwave signals traveling along the line. The amount of dissipated power due to the presence of the electric field in the liquid without ions is given by the Equation [24]:

$$P(x, y, z, f, T) = 2 \cdot \pi \cdot f \cdot \varepsilon'' \cdot (x, y, z, f, T) \cdot |E(x, y, z, f, T)|^2, \qquad (4)$$

in which f is the operating frequency, ε'' is the imaginary part of the complex permittivity of liquid, and $|E(x, y, z)|$ is the magnitude of the electric field strength within the liquid volume. To elaborate more on the operating frequency choice, it is necessary to look into the imaginary part of the complex permittivity of the liquid ε'' and the amount of dissipated power in the liquid volume $P(x, y, z)$, which are presented in Figure 3a,b for the deionized (DI) water case—we are conducting the analysis for DI water as liquid mixtures in biology often have high water content, which has the most dominant influence on the permittivity of mixtures at high frequencies. If another liquid would be chosen (e.g., a solvent in chemistry), the analysis should be conducted starting from the complex permittivity data for the chosen liquid. In the case when the permittivity data is not available, the liquid should be characterized done based on dielectric spectroscopy using commercially available solutions such as coaxial dielectric probes, or in-house developed spectroscopy chips and protocols [25–27].

The imaginary part of the complex permittivity ε'' sets the operating frequency around 20 GHz at room temperature to use the peak of ε'' and have rapid heating at the onset of the heating process. Nevertheless, the product governing heat losses steers the frequency choice in a different direction. If we assume that enough power is available for heating at a frequency range of interest, the operating frequency should be set to the highest possible value. This is concluded by calculating the amount of the dissipated power in a liquid volume having the same electric field strength of 1 V/m at all frequencies—results shown in Figure 3b. The upper limit on the frequency choice in this work is set by available microwave laboratory equipment, and therefore, a frequency of 25 GHz is chosen.
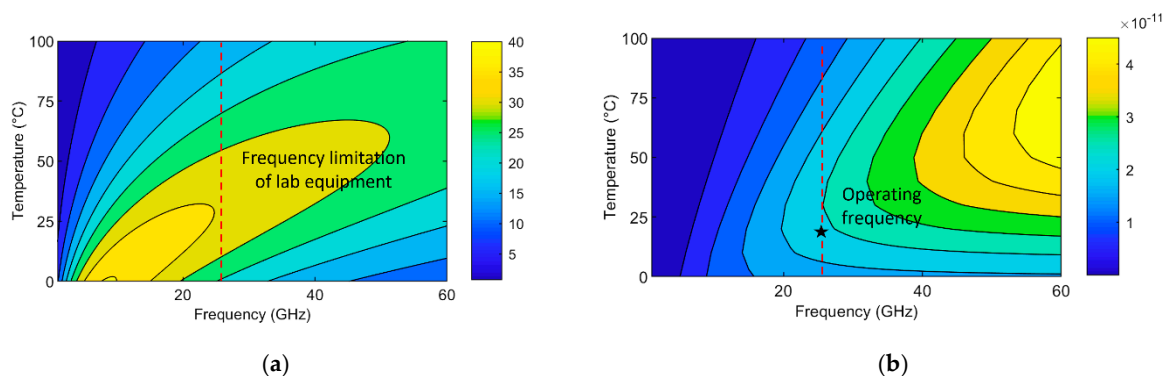

Figure 3. Data used to select operating frequency: (**a**) The imaginary part of complex permittivity of deionized water from 1 to 60 GHz and from 0 to 100 degrees Celsius [28]; (**b**) power losses in deionized water calculated using Equation (4) and the data in Figure 3a for an electric field of 1 V/m at all frequencies.

3. Results

3.1. Heater Design

In the heater design process, it is possible to design the microwave and the fluidic part. Designing the microwave part means sizing the width of the central conductor and the spacing between the central and ground conductors of the co-planar waveguide transmission line. Designing the fluidic part means arranging the layout of the channel in the reaction chamber to further help the heating

uniformity. In the through line design case, the size of fluidic channel sections is kept constant and perpendicular to the transmission line length, as shown in Figure 4a,b. By keeping them perpendicular, the interaction between the electric field and the liquid in the channel is maximized, as previously reported by others [13]. Because the size of the channel sections is kept constant in the through line microwave heater (TLMH) design case, only the microwave transmission line is sized to dissipate equal amounts of power in the liquid located in all fluidic channel sections. This is done in COMSOL Multiphysics (COMSOL AB, Stockholm, Sweden) for 20 channel sections that result in a volume of 465 nL. The total amount of dissipated power is 295 mW for an excitation signal of 1000 mW at 25 GHz—the microwave theory was previously reported [22]. The final design dimensions of the TLMH obtained using COMSOL are depicted in Figure 4c. The TLMH dissipates an average amount of power of 0.63 mW/nL with a variation of 0.066 mW/nL between different sections. All microwave power not transformed into heat goes out at the output port of the TLMH. The electric field strength in the channel shown in Figure 4c is presented for the cross-section A in Figure 4g, 200 μm away from the metal layer of the TLMH, and calculated using an excitation signal of 1000 mW at 25 GHz in COMSOL Multiphysics. This top-view 2D electric field plot provides more insight into the heating uniformity caused by the electric field in the liquid. It shows that the electric field is present in the complete liquid volume with limited gradients along the complete channel length. The side-view plot in Figure 4e for the cross section B, 100 μm away from the edge of the central conductor of the co-planar waveguide transmission line, also shows the 2D spatial distribution of the electric field in the liquid located in the channel and indicates that most of the electric field is contained around the transmission line.
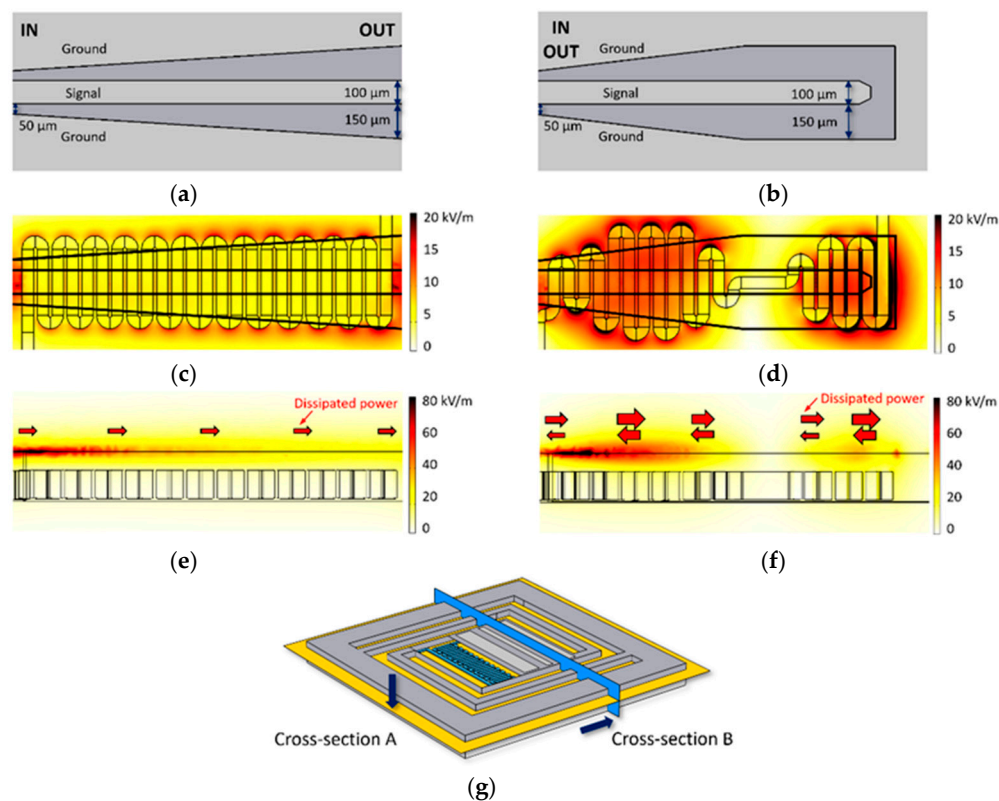

Figure 4. Design of microwave heaters: (**a**) The through line microwave heater (TLMH) with final optimized dimensions; (**b**) the open-ended-line microwave heater (OELMH) with final optimized dimensions; (**c**) the electric field strength for the TLMH at the plane of the cross-section A; (**d**) the electric field strength for the OELMH at the plane of the cross-section A; (**e**) the electric field strength for the TLMH at the plane of the cross-section B; (**f**) the electric field strength for the OELMH at the plane of the cross-section B; (**g**) illustration of cross-sections used for electric field plots.

The open-ended-line microwave heater (OELMH) employs a resonant structure for heating because a standing wave pattern is created. Consequently, the resonant heating structure creates zones without the electric field in which dielectric heating does not occur, while in other zones where the electric field is very strong, fast dielectric heating occurs. Therefore, microwave and microfluidic parts are co-designed together for heating uniformity across the complete liquid volume. The co-design is done by sizing the length of channel sections and spacing between signal-ground conductors to obtain the same normalized dissipated power per unit volume. This can be seen in Figure 4d,f for the final design dimensions of the OELMH—a large volume is present in zones of strong electric fields, while a small volume is present in zones of weak electric fields. Additionally, the spacing between single-ground conductors is smaller in zones of strong electric field than in zones of the weaker electric field. The total OELMH length is chosen to be 3/4 of the wavelength that fits into the reaction chamber. This topology design is also carried out in COMSOL Multiphysics and the obtained OELMH device design results in power delivery of 487 mW to a volume of 315 nL over the transmission line length for an excitation signal of 1000 mW at 25 GHz. The final design dimensions of the OELMH depicted in Figure 4b dissipate an average amount of power of 1.55 mW/nL with a variation between channel sections of 0.46 mW/nL. Once volumes around the minima of the standing wave pattern are excluded from the analysis, 419 mW is dissipated in 241 nL (1.74 mW/nL) with a variation between channel sections of 0.28 mW/nL showing satisfying uniformity of power delivery. The electric field strength in the channel resulting from the OELMH is obtained from COMSOL Multiphysics using an excitation signal of 1000 mW at 25 GHz—it is presented in Figure 4d,f for the cross sections A and B in Figure 4g. The plots presented in Figure 4d,f confirm larger dissipated power than in the case of TLMH due to the presence of stronger electric fields. Additionally, the same plots confirm the larger variation in power uniformity due to the presence of larger electric field gradients than in the case of the through line heater.

3.2. Platform Design

Designed microwave heaters in the transmission line topology are placed on individual reaction chambers depicted in Figure 5a,b, top and bottom view, respectively. Four chambers are put on a single high resistivity-silicon-glass (HR-Si-glass) die that can be integrated with a microwave feeding network, as depicted in Figure 5c, top view. The feeding network is designed with grounded co-planar waveguides to connect the HR-Si die to standard coaxial connectors, as depicted in Figure 5c. Additionally, the ends of transmission lines are intentionally designed to be capacitive to compensate for the additional inductance of the bond wires and minimize reflections. Finally, the designed microwave-microfluidic platform is presented in Figure 5c,d—the microwave and microfluidic part are interconnected from the top side, while the optical access is provided from below. The dimensions of the platform holder in acrylic glass are sized to fit the microscope top stage.
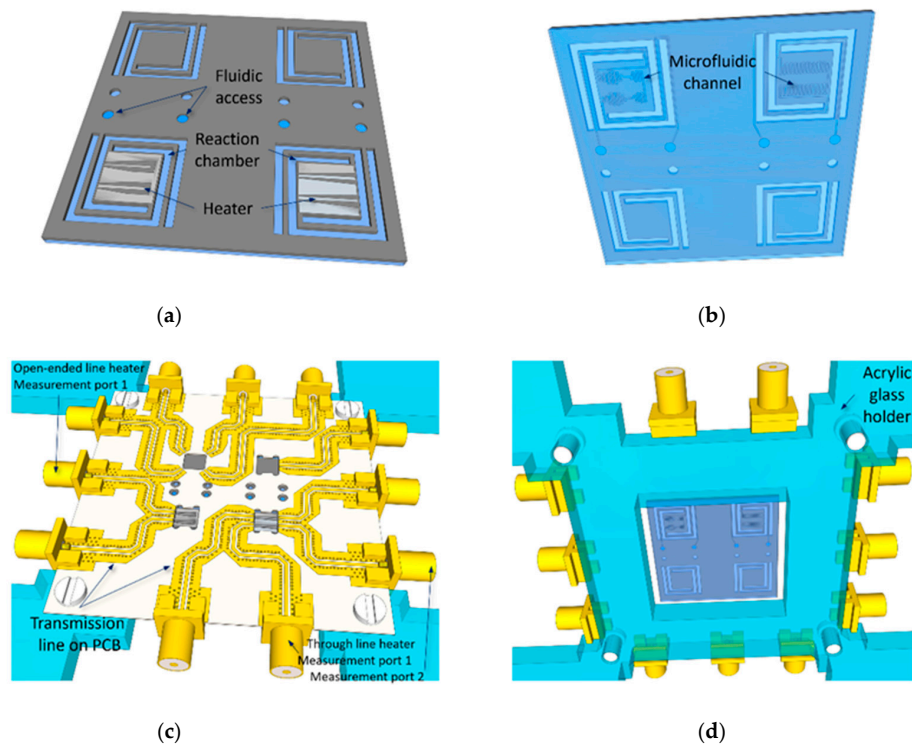
(a)

(b)

(c)

(d)

Figure 5. Integrated heaters on a die with the PCB and the acrylic glass holder: (**a**) The top view of the HR-Si-glass die with four reaction chambers showing microwave heaters; (**b**) the bottom view of the HR-Si-glass die showing microfluidic channels; (**c**) the top view of the integrated HR-Si-glass dies with the PCB and the acrylic glass holder showing feeding transmission lines; (**d**) the bottom view of the integrated HR-Si-glass dies with the PCB and the acrylic glass holder showing the optical access to the microfluidic channels.

3.3. Microwave Measurements

Microwave measurements are often carried out by measuring S-parameters, which represent the ratio of incident and reflected waves at ports of interest [24]. For example, S_{11} is a ratio of a reflected wave at the port 1 and an incident wave at the same port 1, while S_{21} is a ratio of a reflected wave at the port 2 and an incident wave at the port 1. In other words, S_{11} is used to calculate how much power is returned to the source, and S_{21} is used to calculate how much power is transmitted from the port 1 to the port 2 of a device. S_{11} of −10 dB means 10% of the input power is reflected by a device and 90% is delivered to the device. S_{21} of 3 dB means 50% of the incident power passed from port 1 to port 2.

In our case, we measured parameters S_{11} and S_{21}, for ports indicated in Figure 5c. Microwave measurement results of the heaters on an HR-Si-glass die and integrated heaters with the PCB, for the air and deionized (DI) water filled channels are presented in Table 1. The first investigated results are S_{11} parameters of the integrated silicon die with microwave heaters and the printed circuit board (PCB) for the case when the channels are filled with DI water—measurement ports of the die integrated with the PCB are indicated in Figure 5c. In both cases S_{11} is low, which means most of the incident microwave power is delivered to the heating system. Afterward, this amount of the delivered power travels to the heater on HR-Si. While traveling over the feeding transmission line, the microwave signal gets attenuated due to the dielectric and conductive losses of the transmission line on the PCB—this effect can be seen by comparing S_{21} of the TLMH (at the level of the die) and S_{21} of the TLMH integrated with the PCB for the air-filled channel. Additionally, for the OELMH, this can be seen by comparing S_{11} of the heater on the HR-Si die and S_{11} of the integrated die for the air-filled channel. Finally, the power reaching the heaters on HR-Si heats liquid in the reaction chamber, as demonstrated by the heater measurements at the silicon die level for the water-filled channels.

Table 1. Microwave measurement results.

Frequency 25 GHz		TLMH		OELMH
		S_{11}	S_{21}	S_{11}
HR-Si die	Air	−17.74	−0.93	−0.92
	DI Water	−23.57	−2.63	−4.45
Integrated die and PCB	Air	−11.62	−5.26	−4.82
	Di Water	−10.39	−8.55	−16.92

3.4. Heating Experiments

Heating experiments were carried out with 1.58 W (32 dBm) at 25 GHz at the coaxial connector plane on the PCB using the microwave-optical measurement setup [29]—the measurement port 1 is indicated in Figure 5c. Images of the Rhodamine B and deionized water liquid mixture loaded into different reaction chambers before heating are presented in Figure 6a,b. Temperature profiles of the liquid in the channel, calculated based on these images, are presented in Figure 6c,d. The obtained temperature profiles show a spatial temperature variation of ±1 °C, which is the limitation of this measurement technique [30]. Figure 6e–j shows calculated temperature profiles of heated liquid for the first 10 s of heating. It is possible to observe that the liquid mixture is heated uniformly in the first stage of the heating when the highest heating rates are measured. The heating rate and the average temperature of the liquid mixture for two heaters are shown in Figure 6k,l. More specifically, the highest recorded heating rate one second after the heating has started is 16 °C/s for the TLMH and 24 °C/s for the OELMH. A few seconds after the heating has started, the warm liquid acts as a heat source for the HR-Si reaction chamber and the bottom glass substrate, resulting in lower heating rates than in the beginning, as presented in Figure 6k,l. At this point of time, the heat transfer from the heated liquid to the silicon and glass surrounding is highest as the temperature gradient is the largest. The dominant path for the heat losses responsible for the temperature saturation is through the HR-Si substrate due to its thermal conductivity, which is 187.5 times larger than the glass thermal conductivity (150 to 0.8 W/mK). In the end, the system enters the steady state and the liquid does not significantly heat any further, as indicated in Figure 6k,l. The highest measured average temperature is 53 °C for the through line heater and 65 °C for the open-ended line heater.

(**a**)

(**b**)
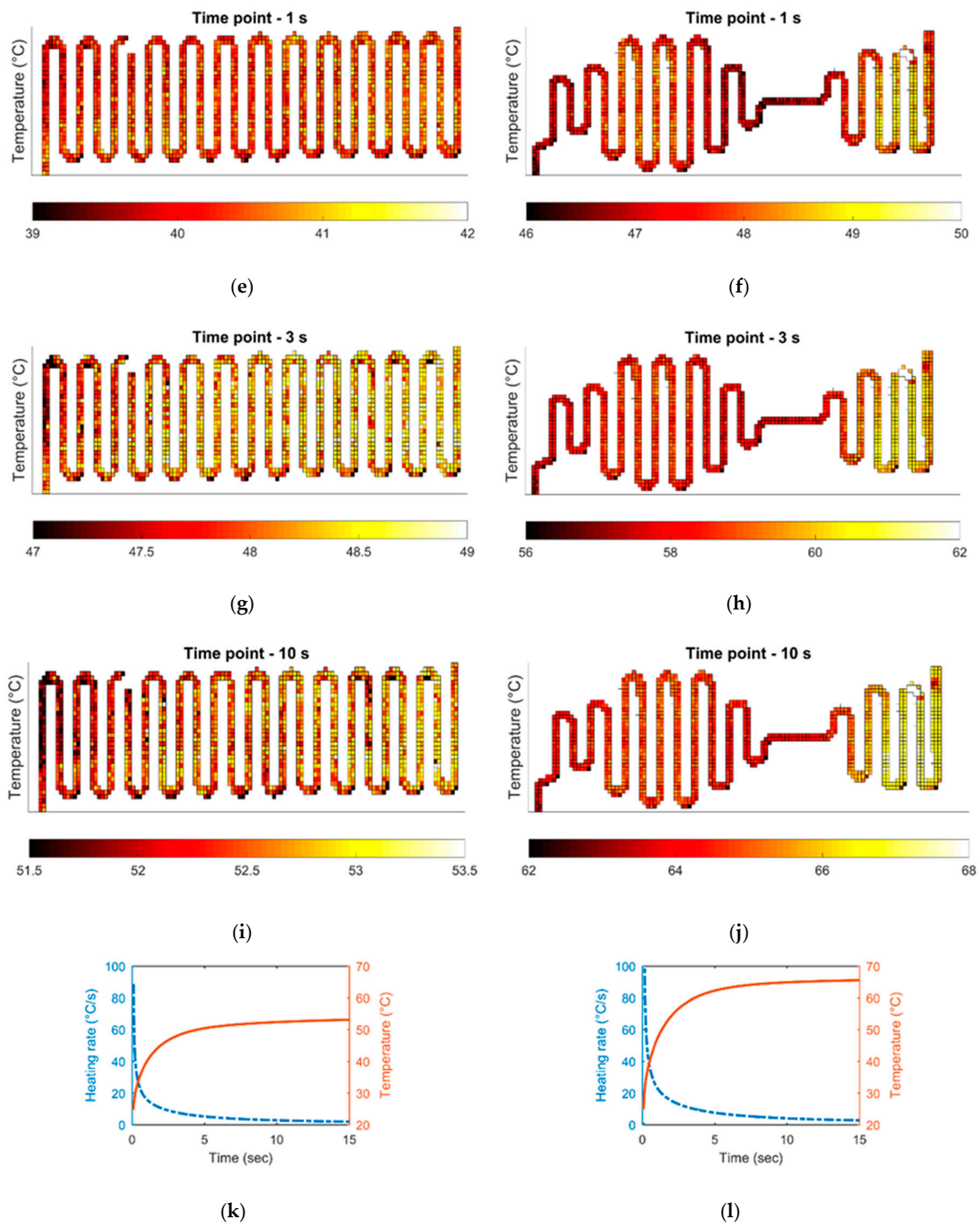

(**c**)

(**d**)
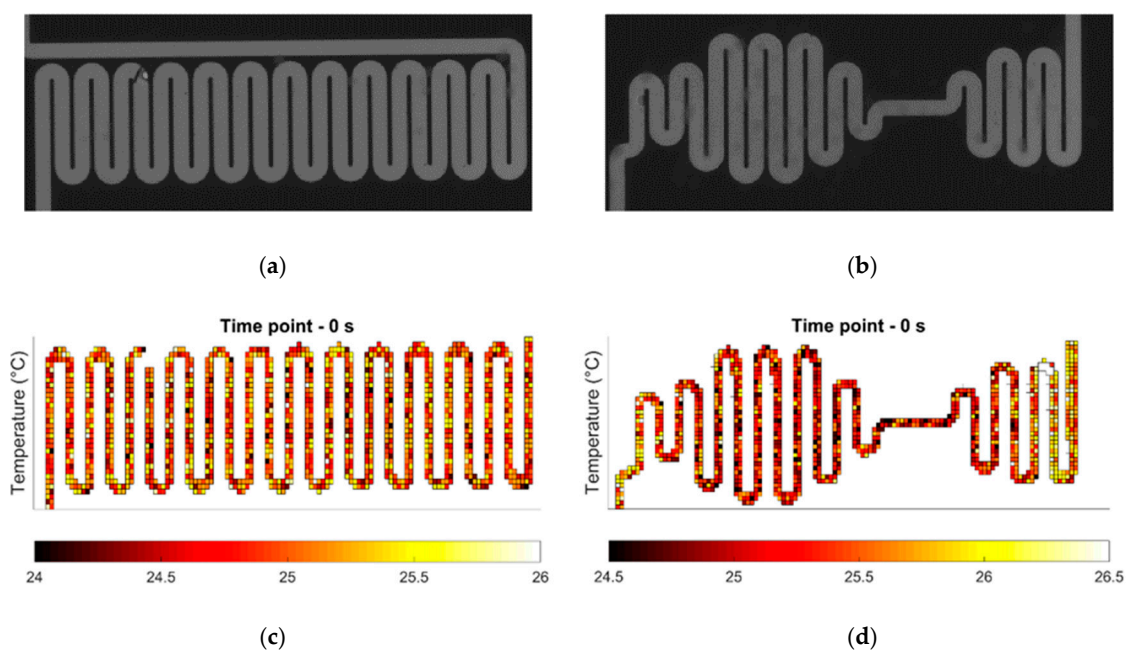
Figure 6. *Cont.*

Figure 6. Microwave heating results: (**a**) Image of the fluorescent liquid mixture located in the channel of the TLMH before heating; (**b**) image of the fluorescent liquid mixture located in the channel of the OELMH before heating; (**c**) the calculated temperature profile of the liquid mixture prior to heating for the TLMH; (**d**) the calculated temperature profile of the liquid mixture prior to heating for the OELMH; (**e**–**j**) the calculated temperature profiles of the liquid mixture during heating for the TLMH and OELMH; (**k**) the calculated average temperature of the liquid mixture and corresponding rate for the TLMH; (**l**) the calculated average temperature of the liquid mixture and corresponding rate for the OELMH.

4. Discussion and Conclusions

The first comparison between the TLMH and the OELMH is based on the highest achieved temperature. According to the microwave design in COMSOL Multiphysics, the OELMH dissipates more power in the microfluidic channel than the TLMH, which is confirmed by microwave measurements—the TLMH dissipates 37% of the input power, while the OELMH dissipates 51% of the input power in the liquid located in the reaction chamber. Therefore, the liquid temperature obtained using the OELMH recorded in heating measurements agrees well with our design results and expectations. The second comparison between the heaters is based on the temperature uniformity of heating. This comparison is possible thanks to the calculated spatial temperature distribution of the liquid in the channel from measurement data. Results in Figure 6c–j show that the TLMH achieves better temperature uniformity at different time points than the OELMH across the whole liquid volume—the temperature uniformity of the TLMH is within ±1.5 °C, while the OELMH shows gradients of ±3 °C. Additionally, the OELMH creates two different temperature zones in its two liquid sections. All these observations in measurement results can be correlated to the 2D electric field distribution presented in Figure 4c,d—the electric field distribution of the TLMH is more uniform once compared to the OELMH. Because of these electric field gradients created by the resonant device, a larger temperature non-uniformity occurs, as reported in Figure 6. Although electric field gradients created by the resonant device result in less uniform heating, the HR-Si substrate helps to locally uniformize the temperature of the loaded liquid due to its high thermal conductivity. In addition, thermally induced flow could also be a factor in uniformizing the temperature. At the end, each heater has its advantages and should be selected accordingly to meet desired specifications.

In summary, this work demonstrates a new class of microwave heaters for sub-microliter volumes in continuous microfluidics for micro total analysis systems. Both types of microwave heaters achieve uniform, contact-less and localized microwave heating without the need for additional microwave structures. This is achieved thanks to the design method that employs a novel co-design of microwave topologies and microfluidic channels, as demonstrated on the design of two different devices. Among many possible modifications of the presented versatile heaters, it is important to stress within the two heating concepts it is possible to adjust channel dimensions to obtain a desired liquid volume, an amount of the dissipated power in liquid to achieve different heating rates over time and the heater-microfluidic system size to fit miniature micro total analysis systems—all parameters often found in specifications of heating systems. Finally, the heating measurement results confirmed the designed behavior of heaters and demonstrated that microwave heating for lab-on-a-chip devices has a large potential in heating applications in cases when a heater cannot be put in the immediate proximity of the liquid and contact between the heater and the liquid should be avoided.

Conflicts of Interest: The authors declare no conflict of interest.

References

1. Ward, K.; Hugh Fan, Z. Mixing in microfluidic devices and enhancement methods. *J. Micromech. Microeng.* **2015**, *25*, 094001. [CrossRef] [PubMed]
2. Yoon, Y.; Kim, S.; Lee, J.; Choi, J.; Kim, R.K.; Lee, S.J.; Sul, O.; Lee, S.B. Clogging-free microfluidics for continuous size-based separation of microparticles. *Sci. Rep.* **2016**, *6*, 26531. [CrossRef]

3. Alves, P.U.; Vinhas, R.; Fernandes, A.R.; Birol, S.Z.; Trabzon, L.; Bernacka-Wojcik, I.; Igreja, R.; Lopes, P.; Baptista, P.V.; Águas, H.; et al. Multifunctional microfluidic chip for optical nanoprobe based RNA detection—Application to Chronic Myeloid Leukemia. *Sci. Rep.* **2018**, *8*, 381. [CrossRef]

4. Curto, V.F.; Marchiori, B.; Hama, A.; Pappa, A.M.; Ferro, M.P.; Braendlein, M.; Rivnay, J.; Fiocchi, M.; Malliaras, G.G.; Ramuz, M.; et al. Organic transistor platform with integrated microfluidics for in-line multiparametric in vitro cell monitoring. *Microsyst. Nanoeng.* **2017**, *3*, 17028. [CrossRef]

5. Bao, J.; Yan, S.; Markovic, T.; Ocket, I.; Kil, D.; Brancato, L.; Puers, L.; Nauwelaers, B. A 20-GHz microwave miniaturized ring resonator for nL microfluidic sensing applications. *IEEE Sens. Lett.* **2019**, *3*, 4500604. [CrossRef]

6. Pan, Y.; Jiang, D.; Gu, C.; Qiu, Y.; Wan, H.; Wang, P. 3D microgroove electrical impedance sensing to examine 3D cell cultures for antineoplastic drug assessment. *Microsyst. Nanoeng.* **2020**, *23*, 6. [CrossRef]

7. Miralles, V.; Huerre, A.; Malloggi, F.; Jullien, M.C. A review of heating and temperature control in microfluidic systems: Techniques and applications. *Diagnostics* **2013**, *3*, 33–67. [CrossRef] [PubMed]

8. Markovic, T.; Bao, J.; Maenhout, G.; Ocket, I.; Nauwelaers, B. An interdigital capacitor for microwave heating at 25 GHz and wideband dielectric sensing of volumes in continuous microfluidics. *Sensors* **2019**, *19*, 715. [CrossRef]

9. Abduljabar, A.A.; Choi, H.; Barrow, D.A.; Porch, A. Adaptive coupling of resonators for efficient microwave heating of microfluidics systems. *IEEE Trans. Microw. Theory Tech.* **2015**, *63*, 3681–3690. [CrossRef]

10. Boybay, M.S.; Jiao, A.; Glawdel, T.; Ren, C.L. Microwave sensing and heating of individual droplets in microfluidic devices. *Lab Chip* **2013**, *13*, 3840–3846. [CrossRef]

11. Issadore, D.; Humphry, K.J.; Brown, K.A.; Sandberg, L.; Weitz, D.A.; Westervelt, R.M. Microwave dielectric heating of drops in microfluidic devices. *Lab Chip* **2009**, *9*, 1701–1706. [CrossRef] [PubMed]

12. Shah, J.J.; Sundaresan, S.G.; Geist, J.; Reyes, D.R.; Booth, J.C.; Rao, M.V.; Gaitan, M. Microwave dielectric heating of fluids in an integrated microfluidic device. *J. Micromech. Microeng.* **2007**, *17*, 2224–2230. [CrossRef]

13. Marchiarullo, D.J.; Sklavounos, A.H.; Oh, K.; Poe, B.L.; Barker, N.S.; Landers, J.P. Low-power microwave-mediated heating for microchip-based PCR. *Lab chip* **2013**, *13*, 3417–3425. [CrossRef] [PubMed]

14. Kempitiya, A.; Borca-Tasciuc, D.A.; Mohamed, H.S.; Hella, M.M. Localized microwave heating in microwells for parallel DNA amplification applications. *Appl. Phys. Lett.* **2009**, *94*, 064106. [CrossRef]

15. Morgan, A.J.L.; Naylon, J.; Gooding, S.; John, C.; Squires, O.; Lees, J.; Barrow, D.A.; Porch, A. Efficient microwave heating of microfluidic systems. *Sens. Actuators B Chem.* **2013**, *181*, 904–909. [CrossRef]

16. Shaw, K.J.; Docker, P.T.; Yelland, J.V.; Dyer, C.E.; Greenman, J.; Greenway, G.M.; Haswell, S.J. Rapid PCR amplification using a microfluidic device with integrated microwave heating and impingement cooling. *Lab Chip* **2010**, *10*, 1725–1728. [CrossRef]

17. Markovic, T.; Liu, S.; Ocket, I.; Nauwelaers, B. A 20 GHz microwave heater for digital microfluidics. *Int. J. Microw. Wirel. Technol.* **2017**, *9*, 1591–1596. [CrossRef]

18. Markovic, T.; Bao, J.; Ocket, I.; Kil, D.; Brancato, L.; Puers, R.; Nauwelaers, B. Uniplanar microwave heater for digital microfluidics. In Proceedings of the 2017 First IEEE MTT-S International Microwave Bio Conference (IMBioC), Gothenburg, Sweden, 15–17 May 2017.

19. Majeed, B.; Jones, B.; Tezcan, D.S.; Tutunjyan, N.; Haspeslagh, L.; Peeters, S.; Fiorini, P.; de Beeck, M.O.; van Hoof, C.; Hiraoka, M.; et al. Silicon based system for single-nucleotide-polymorphism detection: Chip fabrication and thermal characterization of polymerase chain reaction. *Jpn. J. Appl. Phys.* **2012**, *51*, 04DL01. [CrossRef]

20. Duffy, D.C.; McDonald, J.C.; Schueller, O.J.A.; Whitesides, G.M. Rapid prototyping of microfluidic systems in poly(dimethylsiloxane). *Anal. Chem.* **1998**, *70*, 4974–4984. [CrossRef]

21. Bao, J.; Markovic, T.; Brancato, L.; Kil, D.; Ocket, I.; Puers, R.; Nauwelaers, B. Novel fabrication process for integration of microwave sensors in microfluidic channels. *Micromachines* **2020**, *11*, 320. [CrossRef]

22. Markovic, T.; Ocket, I.; Jones, B.; Nauwelaers, B. Characterization of a novel microwave heater for continuous flow microfluidics fabricated on high-resistivity silicon. In Proceedings of the 2016 IEEE MTT-S International Microwave Symposium (IMS), San Francisco, CA, USA, 22–27 May 2016.

23. Markovic, T.; Ocket, I.; Jones, B.; Nauwelaers, B. Contactless microwave heating of continuous flow microfluidics on silicon. In Proceedings of the 20th International Conference on Miniaturized Systems for Chemistry and Life Sciences, Dublin, Ireland, 9–13 October 2016.

24. Pozar, D.M. *Microwave Engineering*, 4th ed.; Wiley: Hoboken, NJ, USA, 2011.

25. Liu, S.; Ocket, I.; Barmuta, P.; Markovic, T.; Lewandowski, A.; Schreurs, D.; Nauwelaers, B. Broadband dielectric spectroscopy calibration using calibration liquids with unknown permittivity. In Proceedings of the 84th ARFTG Microwave Measurement Conference, Boulder, CO, USA, 4–5 December 2014.

26. Barmuta, P.; Bao, J.; Zhang, M.; Marković, T.; Nauwelaers, B.; Schreurs, D.; Ocket, I. Broadband electrical determination of liquid mixing ratios for microfluidics. In Proceedings of the 2019 European Microwave Conference in Central Europe (EuMCE), Prague, Czech Republic, 13–15 May 2019.

27. Liu, S.; Orloff, N.D.; Little, C.A.; Zhao, W.; Booth, J.C.; Williams, D.F.; Nauwelaers, B. Hybrid characterization of nanolitre dielectric fluids in a single microfluidic channel up to 110 GHz. *IEEE Trans. Microw. Theory Tech.* **2017**, *65*, 5063–5073. [CrossRef]

28. Ellison, W.J. Permittivity of pure water, at standard atmospheric pressure, over the frequency range 0–25 THz and the temperature range 0–100 °C. *J. Phys. Ref. Data* **2007**, *36*. [CrossRef]

29. Markovic, T.; Jones, B.; Barmuta, P.; Ocket, I.; Nauwelaers, B. A transmission line based microwave heater at 25 GHz for continuous flow microfluidics fabricated on silicon. In Proceedings of the 2019 49th European Microwave Conference (EuMC), Paris, France, 1–3 October 2019.

30. Shah, J.J.; Gaitan, M.; Geist, J. Generalized temperature measurement equations for Rhodamine B dye solution and its application to microfluidics. *Anal. Chem.* **2009**, *81*, 8260–8263. [CrossRef] [PubMed]